Ultrafast Photo-ion Probing of the Ring-Opening Process in *Trans*-Stilbene Oxide

Matthew S. Robinson,*[a, b] Mario Niebuhr,[a] Fabiano Lever,[a] Dennis Mayer,[a] Jan Metje,[a] and Markus Gühr*[a]

Abstract: The ultrafast photo-induced ring opening of the oxirane derivative *trans*-stilbene oxide has been studied through the use of ultrafast UV/UV pump-probe spectroscopy by using photo-ion detection. Single- and multiphoton probe paths and final states were identified through comparisons between UV power studies and synchrotron-based vacuum ultraviolet (VUV) single-photon ionization studies. Three major time-dependent features of the parent ion (sub-450 fs decay, (1.5 ± 0.2) ps, and > 100 ps) were observed. These decays are discussed in conjunction with the primary ring-opening mechanism of stilbene oxide, which occurs through C–C dissociation in the oxirane ring. The appearance of fragments relating to the masses of dehydrogenated diphenylmethane (167 amu) and dehydrogenated methylbenzene (90 amu) were also investigated. The appearance of the 167 amu fragment could suggest an alternative ultrafast ring-opening pathway via the dissociation of one of the C–O bonds within the oxirane ring.

Introduction

The light-induced ring-opening process of oxirane-based molecules has been studied for over half a century now,[1,2] yet still, there are many unanswered questions relating to a number of processes involved. This includes which bond in the three-membered ring is most likely to be broken, what exact mechanism is followed as the molecule opens up and how different substituents affect the process.[3–6] One molecule which exhibits a number of these issues is the diphenyl substituted oxirane-based *trans*-stilbene oxide (*trans*-2,3-diphenyloxirane), which will be the focus of the study presented here.

It has generally been observed that the primary oxirane molecule, alongside a number of alkyl-substituted oxiranes, undergoes a photo-induced ring-opening process which involves the dissociation of one of the C–O bonds in the oxirane ring.[2,3,7–11] This is in contrast to cyano- and phenyl-substituted oxiranes (such as *trans*-stilbene oxide) which present evidence that the ring-opening process generally occurs through the dissociation of the C–C bond in the oxirane ring instead.[3,12–17] This discrepancy is an obvious curiosity worthy of investigation in and of itself. However, for the next few paragraphs we will focus on the mechanisms that generally occur in oxirane-based molecules after a C–C bond break, as this is the more frequently observed process for our molecule of interest, stilbene oxide. We will lightly touch upon C–O-based mechanisms later on.

In cases in which the ring-opening mechanism of oxiranes proceeds via the C–C bond, Woodward-Hoffman (WH) rules generally describe the process well.[3,4,10,16,18–20] Interestingly, in their seminal papers describing the conservation of orbital symmetry of concerted reactions,[18,19] Woodward and Hoffman themselves explicitly discuss the thermal- and photo-induced ring-opening and closing of oxirane via the C–C bond – despite the C–O bond opening mechanism being the more common pathway for the unsubstituted oxirane molecule.[2,3,7–10] Regarding *trans*-stilbene oxide, WH rules suggest that if it was to open via the C–C bond through thermal means it would do so in a concerted *conrotatory* motion and produce the *cis*-carbonyl ylide (1,3-dipole) seen in route a) of Scheme 1. Conversely, if *trans*-stilbene oxide was to undergo a ring-opening process via the C–C bond through a photo-excited state, WH rules predict it would proceed through a concerted *disrotatory* motion, this time producing the *trans*-carbonyl ylide seen in route b) of Scheme 1.[3,15,17]

Despite this simplified model predicting the primary photo-induced path of stilbene oxide successfully, previously published experimental work presents findings in which additional products have been observed that defy these predictions, whilst theoretical work raises questions as to why this model should be followed in the first place. We will look to discuss these contradictions now.

[a] Dr. M. S. Robinson, M. Niebuhr, F. Lever, D. Mayer, Dr. J. Metje, Prof. Dr. M. Gühr
Institut für Physik und Astronomie
Universität Potsdam
Karl-Liebknecht-Straße 24/25
14476 Potsdam-Golm (Germany)
E-mail: matthew.robinson@cfel.de
mguehr@uni-potsdam.de

[b] Dr. M. S. Robinson
Centre for Free Electron Lasers (CFEL)
DESY
Notkestraße 85, 22607 Hamburg (Germany)

Supporting information for this article is available on the WWW under https://doi.org/10.1002/chem.202101343

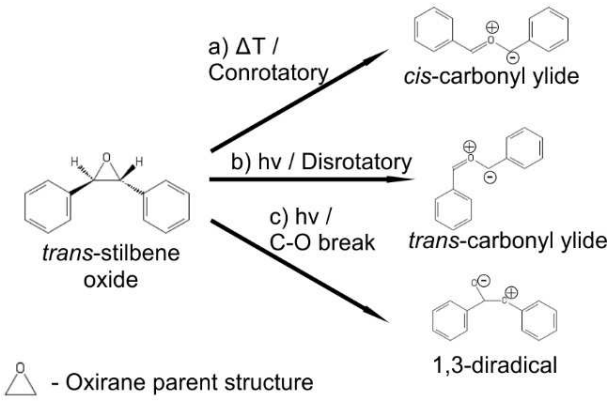

Scheme 1. Diagrammatic representation of the possible ring-opening processes of stilbene oxide, including a) thermal conrotatory opening to produce a *cis*-carbonyl ylide, b) light-induced disrotatory opening to produce a *trans*-carbonyl ylide and c) a potential light-induced ring opening through the dissociation of a C–O bond in the oxirane ring to produce a 1,3-diradical. The basic structure of oxirane is shown for reference.

Friedrichs and Frank performed a number of theoretical calculations to look at the dynamics of both *cis*- and *trans*-stilbene oxide in the first excited state.[3] They performed *full-dimensional* trajectory calculations for stilbene oxide after promoting it to the first excited state, and found that the only products observable were those that move towards a disrotatory ring-opening process after the initial dissociation of the C–C bond of the oxirane ring, that is, in accordance to WH rules. However, when they investigated the *reduced-dimensionality* potential energy surface along the C–C bond direction through linearly interpolated single-point calculations, they could not observe any apparent favorability between the con- and disrotatory mechanisms, despite all of their trajectories following the disrotatory model. These results highlight that whilst WH rules can predict one route over another, we do not fully understand why the disrotatory mechanism is preferred for excited-state stilbene oxide.

From an experimental point of view, picosecond optical excitation experiments by Manring and Peters show that *cis*-stilbene oxide would sometimes lead to products relating to the *trans*-carbonyl ylide (i.e., the symmetry-forbidden product according to WH rules).[20] Other photochemical studies by Lee also show some WH symmetry-forbidden products being formed after the photoexcitation of *trans*-stilbene oxide.[15] In addition, further experiments have observed products that suggest that the ring-opening process is occurring via the dissociation of one of the C–O bonds (as illustrated in route c of Scheme 1),[15,21–23] which is more in line with the process observed in the primary oxirane molecule.[2,3,7–11] All of this suggests that there are multiple potential pathways that stilbene oxide can follow after excitation, and the exact mechanism of these routes is still not yet fully understood.

In an attempt to better understand what dynamic processes may be apparent in stilbene oxide after photo-excitation, we have (to our knowledge) performed the first experiments using *sub-picosecond* pump and probe lasers to study *trans*-stilbene oxide in the gas phase. We are looking to better document the main reaction pathway of *trans*-stilbene oxide after promotion to the first-excited state ($S_1(\pi\pi^*)$, excited with ~266 nm light)[21,23] on the ultrafast timescale, as well as any other competing photo-induced reactions taking place. We performed single-color UV/UV pump-probe ion mass spectroscopy, as this type of spectroscopy has been proved successful in following similar molecular de-excitation paths.[24–26] We excite stilbene oxide with a single photon to the first-excited covalent state and probe the molecule with one or two photons into its ionic states. Parent and fragment ion yield as a function of pump-probe delay allow us to elucidate the dynamics in the intermediate state and relate to possible C–C and C–O dissociation channels. To complement this work, appearance energies of fragment ions have been obtained from vacuum ultraviolet (VUV) dissociative photoionization studies performed at the VUV beamline of the Swiss Light Source (SLS) at the Paul Scherrer Institute (PSI) in Switzerland.[27]

Due to the limitations of the techniques used here, it will not be possible for us to directly elucidate the subtler structural changes of stilbene oxide. Instead, progresses along its excited-state reaction coordinates (i.e., the con- versus disrotatory mechanism), and determination of this is better suited to ultrafast diffraction experiments, as those are already at a level of directly monitoring the ring-opening processes of organic molecules.[28] However, we will nonetheless be able to determine the lifetimes of certain processes unique to the stilbene oxide, as well as comment on larger structural changes in the molecule based on the fragments observed. This work will therefore act as a foundation for future ultrafast studies into this molecule in the femto-/few-picosecond regime.

With respect to the remainder of this paper, full details on the experimental set-ups used for the ultrafast UV/UV pump-probe experiments, as well as the experimental parameters for the VUV photo-fragmentation studies performed at SLS, can be found towards the end of the article in the Experimental Section. In the following, we present the typical photo-fragmentation products observed in the UV/UV and VUV studies. Next, we provide further results from the VUV single-photon fragmentation studies and compare these to the UV/UV multi-photon power-series fragmentation studies to obtain an understanding of the number of photons needed to observe certain fragments. At the end of this section, we focus on examining the time-resolved decays of fragments in the UV/UV pump-probe mass spectra. In the Discussion section, we provide further analysis of these results and what they can tell us about the dynamics of *trans*-stilbene oxide in conjunction with previously published results. Finally, in our Conclusion, we summarize what these studies have elucidated about the photo-induced mechanisms that are likely occurring in stilbene oxide.

Results

We present a typical mass spectrum of stilbene oxide in Figure 1a, which was collected with the UV/UV set-up at time

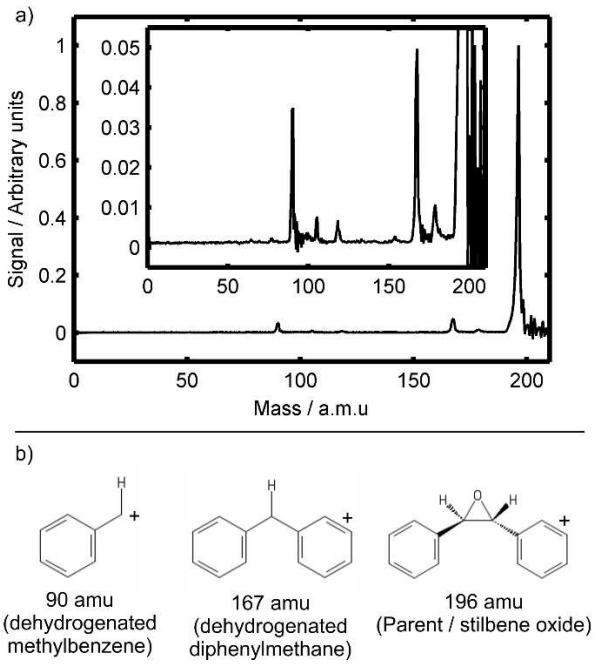

Figure 1. a) Typical mass spectrum observed at time zero in the UV/UV pump-probe experiment. Inset: a magnified version of the same spectrum to highlight the relative strengths of the fragments. b) The predicted structures of the three main fragment ions observed in the mass spectrum.

zero. Several mass fragments can be observed, including those with atomic mass units (amu) of 77, 90, 105, 118, 154, 167 and 178, as well as the parent at 196 amu. In this paper we will focus on the more prominent 90 and 167 amu ions (likely to be dehydrogenated ions of methylbenzene and diphenylmethane, respectively, previously observed from stilbene oxide or similar systems),[21,23,29] as well as the parent ion. The expected structure of all three ions can be seen in Figure 1b.

In Figure 2, we present a summary of the data collected at the VUV end station at SLS using the PEPICO method with a narrow "threshold" electron energy window (see the Experimental Section). Figure 2a, shows a false-color plot of PEPICO events as a function of mass/charge and photon energy. In general, one can identify the same ions along the mass/charge axis of Figure 2a as what was observed in the UV/UV experiment (Figure 1). Figure 2b shows lineouts taken from data seen in Figure 2a for fixed masses, giving the mass-selected threshold photoelectron spectra (ms-TPES).[30] The appearance energies of photo-ions are not affected by the threshold method, however the shape of the presented curves generally differs from non-threshold spectra. The Asher method[31] was used to fit the appearance energies of the fragment ions. Whilst alternative fitting models that take into account a wider range of parameters for more accurate fits are available, such as Rice-Ramsperger-Kassel-Marcus (RRKM) theory and the simplified statistical adiabatic channel model (SSACM),[32,33] approximate energies from the Asher method are sufficient to support the

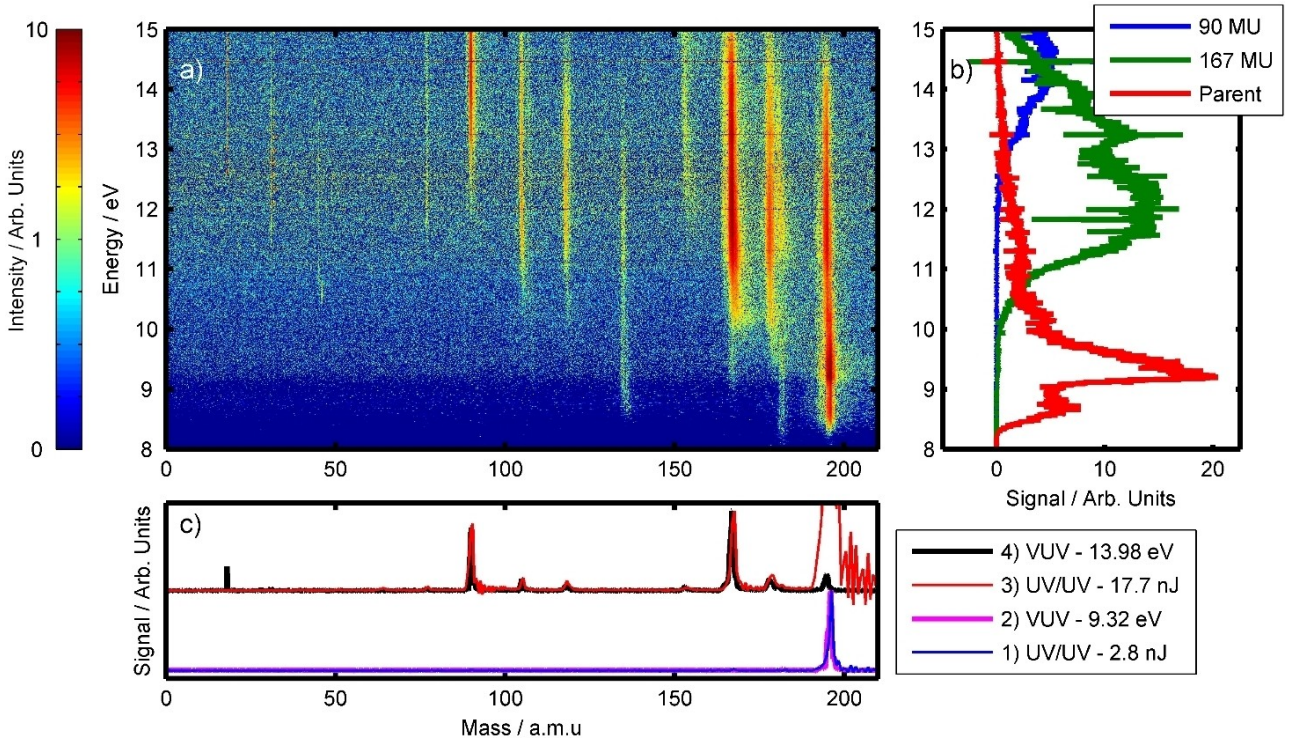

Figure 2. Results from VUV ion mass spectroscopy experiments (collected on a VMI-PEPICO spectrometer) showing a) the overall ion mass spectra for photon energies between 8 and 15 eV in a false color scale with arb. units. b) Cuts along the vertical direction, showing the mass-selected threshold photoelectron spectra (ms-TPES). The sharp peaks are due to experimental artefacts. c) Cuts along the horizontal direction, showing VUV mass spectra at different photon energies and how they compare to low- (lower) and high-power (upper) UV/UV experiments.

UV/UV work presented here. These fits provided values for the parent, and the 167 amu and 90 amu fragment ions as (8.63 ± 0.06) eV, (11.16 ± 0.01) eV and (12.37 ± 0.04) eV, respectively. We suspect that the integrated fragment signals (167 and 90 amu) rise slowly as a function of photon energy, due to internal thermal energy stored in the exited molecule. This, however, will be further elaborated on in a publication dedicated to the full VUV results of stilbene oxide.

These appearance energies suggest that two photons of 266 nm light (i.e., 2 × 4.66 eV) are sufficient to create the parent, whilst three are necessary for the 90 or 167 amu fragments. To further support this point, Figure 2c shows direct comparisons of the mass spectra between the two different experiments under different regimes. The lower part shows a UV/UV produced mass spectrum (1) in addition to the SLS experiment at $h\nu = 9.22$–9.42 eV (2). The UV/UV experiment is set at time zero (see the Experimental Section), using relatively low pulse energies (a combined 2.8 nJ). This is a regime where we expect two-photon processes to be dominant. Similarly, the upper half of Figure 2c compares (3) the UV/UV pump-probe experiment at time zero performed with higher powers (a combined 17.7 nJ) and (4) the VUV experiment integrated over the range of 13.88–14.08 eV. The UV power is in a regime where we expect three photon transitions to be dominant.

These plots in Figure 2c do show strong correlations between their respective pairings (i.e., between plots 1 and 2, as well as between 3 and 4), with the same fragments appearing in each of them and the relative ratios of the peak heights among the two experiments being approximately the same, supporting the idea that the parent ion and the fragment ions are produced through two- and three-photon processes, respectively, in the UV/UV experiment. The biggest discrepancy is the difference in the parent ion signal in plots 3 and 4. This can be explained by the inhomogeneity of the laser focus. Whilst the inner part of the focus will be at a high intensity and therefore likely to produce three-photon process, the outer part of the focus, with lower intensity, will likely favor up to two-photon processes, and hence a sufficient parent signal remains in the UV/UV experiment.

In addition to the attribution of fragments to specific multi-photon processes given above, we determined power dependencies of the parent and most prominent fragment ions (Figure 3). The following experiment is analogous to the seminal power-dependency experiments by L'Huillier et al., which investigated singly and doubly ionized xenon ions produced via both nonresonant multiphoton ionization and resonance-enhanced-multiphoton ionization (REMPI) of Xe atoms.[34] The power of the pump and probe beams were changed simultaneously by adjusting the conversion efficiency of the THG set-up by rotating the $\lambda/2$@800 nm waveplate that sits before said THG set-up in front of it. Experiments were performed over eleven different combined pulse energies between 0.94–17.95 nJ (as measured on the power meter behind the laser-molecule interaction region with both beams on the detector). To test if the power series is pump-probe delay-dependent (in a similar fashion to the work of Koch et al.),[35] data were recorded for four different pump-probe delays (time zero, 100, 1000 and 10000 fs), with data from 40000 individual shots of the laser being recorded on the oscilloscope for each data point. For each ion of interest, it was possible to perform linear fits to the $\log_{10}$ values of the signal strength and combined pulse energy, and extract a slope for each time delay, the results of which can be seen in Table 1.

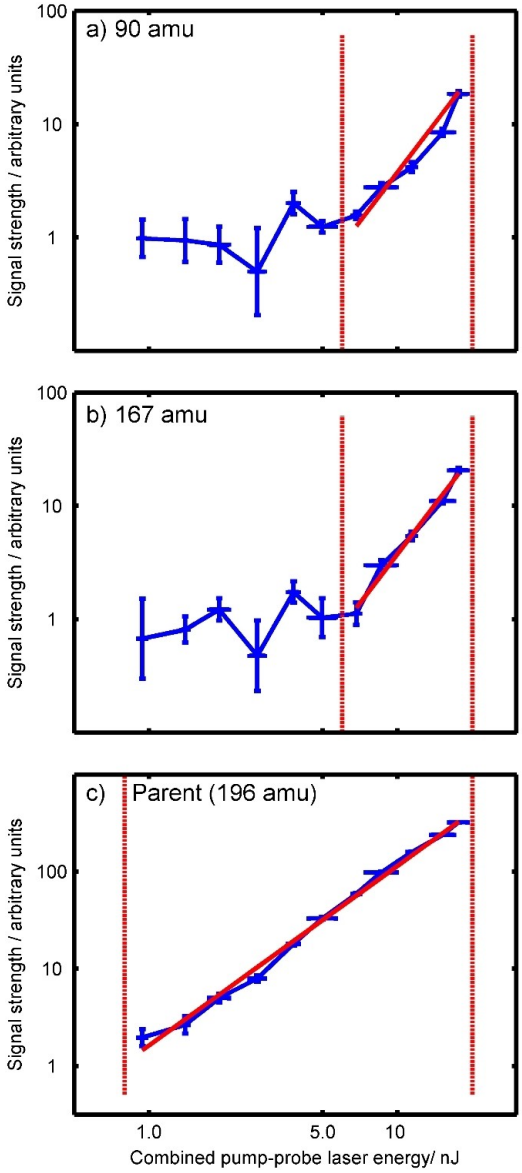

Figure 3. Plots depicting the signal-to-pulse-energy dependence of the a) 90 and b) 167 amu fragments and c) the parent ion as observed at the time-zero overlap. Solid red lines show the fitted slopes. Dotted red lines show the region over which the slopes are calculated. For the parent ion, we found a slope close to 2; for the two fragment ions, the slope is close to 3 (see the text).

These linear fits provide additional support for the number of photons absorbed to produce a certain ion. The slope fitted for the parent ion for all pump-probe delays have an average value of (1.9 ± 0.1) suggesting a two-photon ionization process at all of the measured time delays. With the 90 and 167 amu fragment ions, fits were performed over a narrower pulse

Table 1. Slopes and error of $\log_{10}$(signal) vs. $\log_{10}$(power) plots for associated masses. The slope for the parent ion was calculated over pulse energies between 0.94 and 17.95 nJ, whilst for the fragments the range was 6.80–17.95 nJ.

Delay time [fs]	90 amu slope	167 amu slope	Parent slope
0	2.41 ± 0.28	2.88 ± 0.20	1.85 ± 0.05
100	2.77 ± 0.42	2.80 ± 0.26	1.88 ± 0.06
1 000	2.58 ± 0.21	2.71 ± 0.11	1.95 ± 0.03
10 000	2.14 ± 0.38	2.55 ± 0.27	1.85 ± 0.05

energy range of 6.8–17.95 nJ, as pulse energies below 6.8 nJ were not able to produce sufficient signals above the noise level. The average of the fitted slopes was calculated to be (2.5 ± 0.3) and (2.7 ± 0.2), for the 90 and 167 amu fragments, respectively, suggesting that these fragments are produced in higher-order (likely three-) photon processes. Due to the relatively low intensities used and the poor absorption efficiency of the S_1 state of stilbene oxide,[22] we believe that we are in the regime where the excited state is not saturated, and hence the photon-orders presented above accurately represent the number of photons needed to ionize the molecule from the ground state.[34]

We now present the time-resolved data. Figure 4 shows pump-probe data from −500 fs to 5 000 fs with the step size ranging from 12.5 to 500 fs depending on the delay range. In these experiments an averaging mode on the oscilloscope was used, where 1 000 shots from the 1 kHz repetition rate laser were averaged to form a single trace. For each data point, 120 seconds' worth of traces were then collected in a delay-randomized manner, before averaging the data further during analysis. Due to the strong differences in signal strength between the parent ion and the fragment ion, data was collected in two separate runs with different gain settings on the oscilloscope. In the first, the gain was optimized for parent ion (i.e., strong, but not saturated), and in the second the gain was optimized for the fragments settings (i.e., parent saturated). All other experimental parameters were kept the same. The area under the peak of each ion of interest was integrated and plotted as a function of time, and can be seen in Figure 4, with the error bars representing the standard deviation observed over the 120 one-second-long collected traces. Unfortunately, due to the nonlinear scaling between the two gain settings, it is not possible to make accurate time-dependent ratio comparisons between the parent ion and the fragment ions. The time-dependent fragment specific plots seen in Figure 4 collected using a single gain setting will not suffer from this issue. Further data were collected between −1 and 100 ps (with step size ranging from 50 to 10 000 fs depending on the delay range), yet it was found that for all ions the only signal after ~3 ps was a slow decay that continued outside of the scan range, and remained significantly above the combined pump-only-plus-probe-only background signal (blue line in Figure 4). Because of this, only data from −0.5 to 5 ps is presented here.

Figure 4c) shows a fast feature exhibited by the parent ion around time zero. As one can see, this feature appears within the time interval of ~75 fs either side of time zero and is

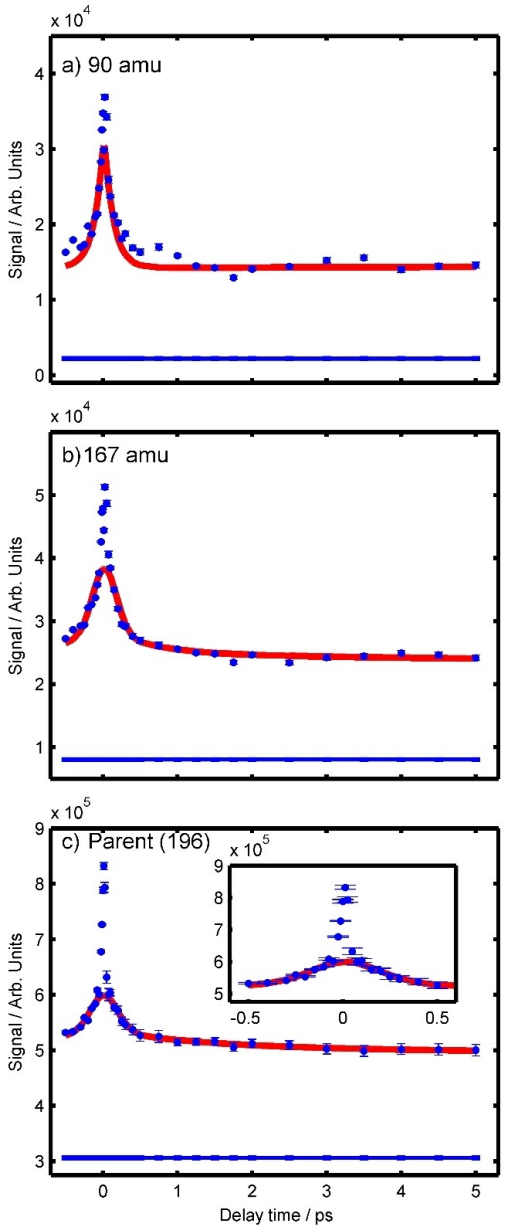

Figure 4. Time-dependent decay signals for the a) 90 and b) 167 amu fragment ions, as well as c) the parent ion (the inset highlights a tall sub-autocorrelation feature). The original data can be seen as individual blue points, and the fit as a red line. Below each decay plot is the summed signal (blue lines) obtained from the summed pump-only and probe-only experiments, highlighting that the time-resolved experiments produce a signal that is long lived compared to the 5 ps scan interval.

therefore significantly shorter than the 300 fs pulse duration predicted by the autocorrelation studies discussed in the Experimental Section. Similar features, albeit weaker, can be seen for the fragment ions as well (Figure 4a and b). We will review this phenomenon extensively in the Discussion section.

Excluding the data points in the first ~75 fs around time zero, we fitted the data and determined a number of decay constants from the time-resolved observations. For the slow decay dominant after ~3 ps, we fitted a simple exponential decay with time constant τ_3 to all ions of interest. These fits

Table 2. Fitted values (and errors where applicable) for the decay times of the ions observed.

Ion	τ_1/fs	τ_2/fs	τ_3/fs
90 amu	tends to zero	740 ± 430	412 000
167 amu	tends to zero	680 ± 280	179 000
parent	tends to zero	1 520 ± 230	791 000

gave τ_3 as being greater than 100 ps for all fragments (see Table 2 for exact values), each with large errors (not detailed). These large errors are due to a combination of scattered data points and short delay range of 100 ps. We therefore simply state that $\tau_3 > 100$ ps. For the time-resolved signal that lies within the first 3 ps, the data were fit to a Gaussian convoluted with three decaying exponential functions.[26,36] To account for the respective two- and three-photon natures of the parent ion and its fragment ions, respectively (as suggested by the results from the power series), the FWHM of the Gaussians used were based on auto-correlation signals of 1,4-dioxane (two-photon ionization, 430 fs) and xenon (three-photon ionization, 370 fs). These signals were obtained using the same pump-probe conditions used to study stilbene oxide (see the Experimental Section). In each fit, the amplitudes and decay constants for two of the three decaying exponentials convoluted with the respective Gaussian were allowed to refine freely after providing a suitable estimate. For the third decaying exponential, the decay constant, τ_3, was fixed to the value obtained from the fit of the "slow decay" discussed previously, whilst the amplitude was allowed to refine freely (after an initial estimate). Refinement of the time-zero position was also performed to improve the fits. In addition, loose refinement of the FWHM of the Gaussian was also allowed in initial fits, however, its value never changed by more than a few fs outside of what was predicted by the aforementioned auto-correlation experiments, and so was ultimately kept fixed. For completeness, alternative fits using two or four exponentials were tested, however, it was found that the two-exponential fit could not suitably describe the data. In the case of the four-exponential fit, we would either observe two of the decay constants converging to the same value, or for one of the amplitudes of the exponentials tending to zero.

We found that the value for the first decay constant, τ_1, tended towards zero (whilst keeping its amplitude) for all ions. This suggests that the signal seen in the first few hundred femtoseconds primarily consists of the auto-correlation signal of the pump and probe beams with little contribution/modulation provided by the response of the molecule. What this means exactly for the dynamics of stilbene oxide will be discussed in the next section. For τ_2, we fitted values of (1520 ± 230) fs, (680 ± 280) fs and (740 ± 430) fs for the parent, 167 and 90 amu ions, respectively. The final fit for each ion of interest can be seen in Figure 4, and summaries of all the fit values can be seen in Table 2.

Discussion

Starting with the combined results of the VUV-determined appearance energies and the UV/UV power series, we show that the parent ion signal is two-photon dominant, and the fragment ions three-photon dominant with respect to 266 nm light for the pump-probe delays investigated. This suggests that the time-dependent parent ion signal seen in Figure 4c is the result of a [1 + 1′] REMPI process. This provides us with confidence that the measured time-resolved results relate to the molecular dynamics after its initial excitation to the S_1 state by a single photon from the pump beam, before it is ionized by a second photon from the probe beam.

For the three-photon-dependent fragment ions, both [1 + 2′] and [2 + 1′] REMPI processes are possible. If the time-resolved signal was coming from a [1 + 2′] REMPI processes, this would suggest that the time-resolved signals relating to the fragment ions seen in Figure 4a and b would also be linked to the initial excitation to the S_1 state. However, a [2 + 1′] dominant REMPI processes would instead suggest that the dynamics are related to the cation. Whilst we suspect that we have been working at low enough pump powers to favor one-photon excitation, and hence the [1 + 2′] REMPI process, the data available here does not allow us to confirm this. Therefore, this limits what conclusions we can draw about the molecular dynamics from the fragment ions.

Moving the discussion to the time-resolved results, we first focus on the tall, temporally short signal seen for the parent ion. The feature cannot be explained by a higher order process, as we did not identify any such process in the power scans or comparisons to the VUV data.

To help us understand this feature, we turned to similar, previously published studies. Recent pump-probe photoelectron investigations by Kotsina et al. have shown that when probing molecules with states that possess a lifetime shorter than the duration of the laser pulse used to investigate it, one can still observe a signal from this state, but it will be significantly under-sampled compared to longer-lived states within the same system.[37,38] This led us to believe that the tall, narrow feature seen in Figure 4 could potentially be due to under-sampling a very short-lived state in stilbene oxide. To test this hypothesis, we performed a series of simulations, that are described extensively in the Supporting Information. In short, the simulations highlighted two main results. If one under-sampled a decay that was longer than the auto-correlation function of the pump and probe beams, the overall signal will to a large degree look like the well-sampled signal, just with significant noise on top of it. However, if one under-sampled a decay that was shorter than the auto-correlation signal, then a tall, narrow spike, much like what is seen in Figure 4, is seen to sit on top of what could be considered to be a noisy variant of the well-sampled signal. From these simulations, several items could be taken away.

First, the simulation showed that outside of the tall, under-sampled feature, the signal observed matches well to the auto-correlation signal/the remaining exponential decays convoluted with the auto-correlation (especially when $\tau_i >$ auto-correlation

length). This gives confidence that the fits which we made to the data presented in Figure 4 – which excluded data points related to the under-sampling spike – are suitable.

Second, the similarity between the tall, narrow feature around time zero that is seen both in Figure 4 and the simulations of an under-sampled decay that is shorter than the auto-correlation signal, suggest that stilbene oxide likely has a sub-autocorrelation feature that is being under-sampled in this experiment. However, the exact duration of this feature is obscured by the auto correlation itself, and therefore in order to better understand it, one would have to use much shorter probe pulses than what has been used here.

With all of this in mind, we therefore have evidence for three individual ultrafast decays for the parent ion of stilbene oxide, which we will now look to interpret; τ_1 (sub-autocorrelation), τ_2 (1.5 ps) and τ_3 (100 + ps).

Long-lived decays of several 100 ps, like that seen for τ_3, are usually related to long-lived triplet states decaying into the "hot" ground state[39] or dynamics of the "hot" ground-state population itself.[40] Based on our results alone, we cannot distinguish between these two processes. However, previous publications point towards ground state dynamics. First, triplet states of oxirane-based molecules have been suggested in the past, however these have generally been reached through the use of photosensitizers (using >300 nm photons) rather than direct excitation, and have generally resulted in a higher mix of symmetry-forbidden products observed with nano-to-micro-second lifetimes.[15,41] This excludes the triplet path. Second, photolysis experiments of *trans*-stilbene oxide by Manring and Peters showed that the *trans*-ylide would appear ca. 400 ps after excitation by a 266 nm light source, and generally only produced the symmetry-predicted products.[20] This similarity between this result and the value of τ_3 strongly advocates that through τ_3 we are tracking the production of the *trans*-ylide via the hot ground state.

The fits to the data of the parent ion signal seen in Figure 4c suggest that there are two ultrafast decays – one that is on the order of 1.5 ps (τ_2) and one that is faster than the auto-correlation (ac) of the pump and probe beams, which we now refer to as the "sub-ac" decay (τ_1). Unfortunately, there is little literature information about molecular processes of stilbene oxide on this timescale. The fastest experiment we know of is the aforementioned study by Manring and Peters, which utilized a 25 ps laser.[20] Theoretical work by Friedrichs and Frank suggested that after promotion to the first excited state, the C–C bond in the oxirane ring is quickly broken within the first 50 fs. This would fit to the short sub-ac (τ_1) time constant. Timescales on following events are less clear.[3] By looking at the rotation direction of the phenyl rings after excitation, Friedrichs and Frank state that they are able to confirm that excited *trans*-stilbene oxide tends towards the disrotatory product. However, information in the publication only shows dynamics up to 250 fs after excitation. Unfortunately, we could see no information as to if their calculations continued on after this point, and so it is difficult to directly attribute τ_2 to anything seen here based on these results.

The appearance of the 167 amu fragment is interesting in its own right, as it may be an indication of a reaction which starts with the breaking of one of the C–O bonds in the oxirane ring (as depicted in Scheme 2), instead of the C–C bond. If this C–O break is initiated by the promotion to the first excited state, this fragment may confirm the idea that *trans*-stilbene oxide may have multiple reaction pathways in the first-excited state.[21–23] In order for the 167 amu fragment to form, a 1,3-diradical will likely be produced as an intermediate due to the photo-dissociation of the C–O[5,11] This intermediate can then undergo a 1,2-migration of one of the phenyl groups and eject an aldehyde group.

We support this pathway by two arguments. First, if the ring-opening process was to occur exclusively via the initial dissociation of the C–C bond in the oxirane ring, the two phenyl groups would be forced apart from one another as the C–O–C bond likely relaxes. This would make it difficult for the methylphenyl radicals to recombine after one of the C–O bonds break, as the group would likely be ejected away from the rest of the molecule. This argument is further supported by past studies which show that appearances of *trans*-stilbene from photo-excited stilbene oxide is not due to the recombination of radical methylphenyl groups. This point is strengthened by that fact that these studies were performed in solution[23] offering even the possibility of geminate recombination.[42] Second, it is already well known that the breaking of one of the C–O bonds is the preferred process in the parent oxirane molecule, and that this is generally followed by the 1,2-migration of a hydrogen atom within the molecule (known as the Gomer-Noyes mechanism).[2,3,5,8,43] Whilst the migrating fragment here is much larger, the 1,2-migration of phenyl groups has been observed before in similar 1,3-diradicals,[29] as well as the more common 1,2-migration of alkyl groups in other oxirane based molecules.[5,11]

The 167 amu ion also appears in the VUV experiment at photon energies higher than 11.16 eV. Therefore, a similar mechanical process as to what has been suggested here must also occur in the single-photon VUV experiment in order for it

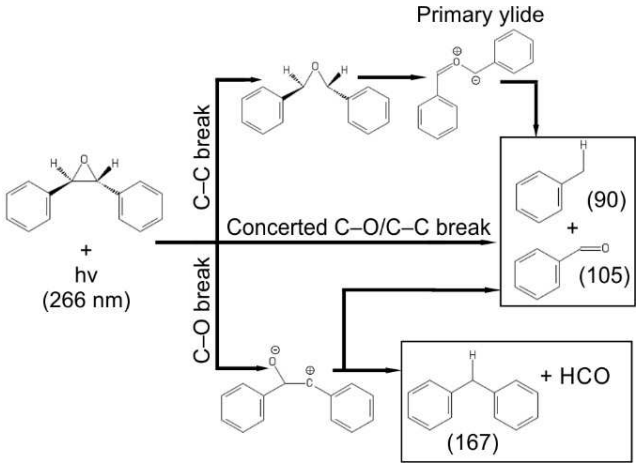

Scheme 2. Possible one-photon-induced reaction pathways that produce the 167 and 90 amu fragments.

to be observed. We therefore cannot rule out, that the C–O bond break occurs in the ionic states, nor whether the dynamics visible in this channel occurs on the neutral or parent cation states without the involvement of the C–O bond.

We now discuss the formation of the 90 amu fragment (Scheme 2). This fragment could appear after separating itself from the parent molecule by breaking one of the C–O bonds once the parent structure has undergone the expected excited-state disrotatory ring-opening process via the initial breaking of the C–C bond. However, alternative routes to producing this fragment are possible. One path could proceed via an *initial* C–O bond break forming the 1,3-diradical (as previously suggested for the 167 amu). This diradical can decay into the 90 amu fragment accompanied by a 105 amu fragment through the dissociation of the C–C bond of the former oxirane ring (Scheme 2). Another path could involve the concerted dissociation of the C–C bond and a C–O bond in the oxirane ring to produce the 90 amu fragment in a single step. Interestingly, past theoretical work by Bigot et al. suggest that all three fragmentation mechanisms were possible for the oxirane parent molecule,[10,44] and have been discussed in relation to stilbene oxide by Lipson et al.[21]

With respect to the dynamics visible through the 90 and 167 amu fragment ions, we see three similar decays in each fragment. The τ_1 is a sub-ac decay, τ_2 is an approximately 700 fs and τ_3 is once again a 100+ ps decay. It is tempting to say that they share a common one photon-induced dynamical pathway, which would likely be the one initiated by the initial breaking of the C–O bond in the oxirane ring. However, in the end we do not have sufficient evidence from this experiment, other ultrafast studies, nor theory to fully support this model. Interestingly however, one can note oscillations in the slow decay (i.e., >1 ps) of the 90 amu fragment ion. It is possible that these oscillations are due to vibrations upon the excited state before photons from the probe induce ionization/dissociation. However, due to the multiple ways the 90 amu fragment is formed, and our uncertainty as to which path is dominant, it is hard to say exactly what this possible vibration could be related to. The fact though that this oscillation is only observed for the 90 amu fragment ion, may be an indication that it is produced through a different mechanism than the 167 amu fragment ion.

Although there is evidence to show that most of the products that we have observed here have been observed before in other UV single-photon excitation experiments,[21–23] it is difficult to directly attribute this to dynamics on the first excited state. This is because whilst we have shown they appear via a three-photon process, we cannot say as to if these fragments are appearing due to dynamics occurring via a [1+2′] REMPI process (i.e., on the neutral excited state) or via a [2+1′] REMPI process, which would likely launch a vibrational wavepacket on the ground ionic state with about 1 eV excess energy. This could also lead to an ultrafast vibrational relaxation out of the Franck-Condon region. Thus, we cannot rule out a [2+1′] process. However, we would like to note that although it appears with a weaker signal than the 90 amu, the appearance of the 105 amu fragment (i.e., the counterpart to the 90 amu fragment, as seen in Scheme 2), may be an indication that fragmentation is indeed taking place in the neutral state after excitation, and before the probe pulse arrives. If we are indeed observing a [1+2′] REMPI process with respect to the fragments, the shorter τ_2 decay value observed for the fragments compared to the parent, could be an indication of subtleties between the final cationic states used for probing. It could suggest that the band gap between the neutral excited state and the ionization states that produce the fragments is growing faster than the gap between the neutral excited state and the ionization states that produce the parent ion.

Conclusion

The results presented here provide new information about the photo-induced dynamics of stilbene oxide, but they also raise a number of questions as to what is actually happening within the molecule on the ultrafast timescale after excitation. We observe three decay constants for the parent ion. The similarities between our longest decay time (i.e., $\tau_3 = 100+$ ps) and the appearance time of the ylide state observed by Manring and Peters[20] indicate decay to the ylide states. For the faster decay constants, any attribution to C–C bond breaking and the initial rotation of the phenyl groups remains speculative, as we are unable to confirm the root of the first two decays without further information from additional ultrafast experiments or extended theoretical studies. The best that we can claim is that there is likely a rapid movement out of the Frank-Condon region within in the first 450 fs after excitation, followed by a longer decay of ~1.5 ps of unconfirmed origins.

The appearance of the 167 amu ion might point towards a secondary ring-opening mechanism that involves the intial breaking of the C–O rather than the C–C bond. If this occurs in the neutral excited state, it might confirm the idea that the S_1 can exhibit different ring-opening mechanims. However, at this stage, we are unable to claim definitively whether the underlying dynamics in this fragment are dependent on single- or multiphoton excitation.

Nonetheless, the results presented here provide a starting point for future ultrafast experiments and further dynamic theory studies in an effort to better understand the novel dynamics of stilbene oxide.

Experimental Section

UV/UV-ion mass spectroscopy: Figure 5 shows a schematic of the experimental set-up used in the time-resolved UV/UV pump-probe ion mass spectroscopy experiments. The 35 fs output of a 1 kHz Ti: Sapphire regenerative amplifier, with a central wavelength of 800 nm, is directed through a collinear third-harmonic generation (THG) set-up, consisting of two BBO crystals, a calcite delay-compensation plate, and a zero-order $\lambda/2$@800+λ@400 nm waveplate. The output power of the THG (266 nm/4.66 eV) is controlled by rotating the angle of a zero-order $\lambda/2$@800 nm waveplate that is situated before the THG set-up. The remaining 800 and 400 nm light is filtered out by a number of dichroic mirrors and wavelength-specific high reflectors between the THG set-up and the sample. The 266 nm light is directed through a Michelson

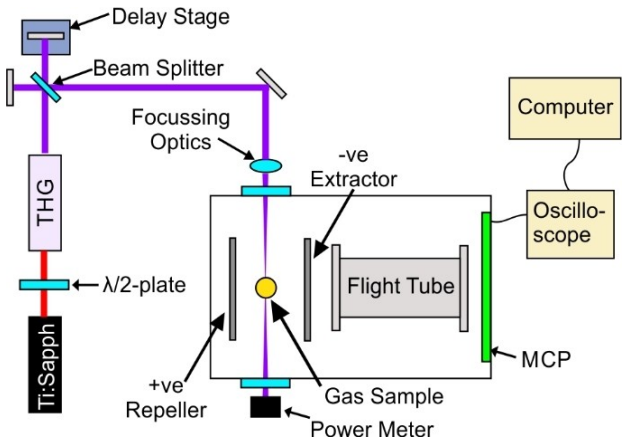

Figure 5. Schematic of the experimental set-up, showing the path of the laser from the Ti:Sapphire laser through the Third Harmonic Generation (THG) set-up, into the Michelson Interferometer before being directed into the ion mass spectrometer, where ions are created and their time of flights recorded.

interferometer to produce the necessary pump and probe beams, with a translation stage located in one arm to allow for a variable delay between the two beams. The UV light is then focused into the gas target within a vacuum chamber, and monitored by a power meter behind the exit window of the vacuum chamber. The beam pointing is actively controlled by a virtual-focus-feedback system.

For the majority of the experiments described, the combined pulse energy of the two UV beams was measured behind the chamber as 10.2 ± 0.2 nJ, unless stated otherwise (e.g. in the UV/UV power scans), with an approximate 50/50 split in terms of energy between them. The focal diameter of the UV beams was measured to be approximately 30 μm (FWHM) at the sample, providing an intensity of about 2.5×10^9 W/cm^2 per laser pulse.

We use a Wiley-McLaren mass-spectrometer set-up[45] and a multi-channel plate (MCP) detector coupled to an oscilloscope to read out the time-of-flight traces. All data from the oscilloscope is then transferred to a computer, where all traces are recorded. The interaction region sits symmetrically in a repeller-extractor field with $+900$ and -900 V respectively on each electrode, situated 30 mm apart. The 180 mm long flight tube starts 10 mm behind the extractor and is set to -1600 V to further accelerate the ions. Voltages on each component were slightly tuned while keeping differences constant to optimize resolution. The mass resolution of the spectrometer with the current digitizer settings was about 150. For each data point with light (i.e., where the laser was allowed to enter the chamber), a "dark" spectrum was also recorded (i.e., where the laser was blocked to record a background signal). Pump-only and probe-only signals were also collected alongside the main experiment to help with background analysis.

The pulse duration of the UV laser was obtained by recording the time-resolved mass spectra of different gases backfilled into the apparatus via a needle valve, the opening of which was situated near the focus of the pump and probe beams. The gases used were 1,4-dioxane and xenon, which are ionized via a two- and three-photon nonresonant process, respectively, when using 266 nm photons.[46,47] By recording how the parent ion signal of both samples varied with respect to the pump-probe delay it was possible to measure the auto-correlation values for the pulses. A FWHM of (430 ± 10) and (370 ± 10) fs, was measured for the 1,4-dioxane and xenon, respectively, both of which suggest a pulse duration around 300 fs. Interference fringes among pump and probe pulses are not completely averaged out by interferometer instabilities over the measurement intervals. This point is addressed further in the Discussion section.

Trans-stilbene oxide, obtained from Sigma-Aldrich (purity 98% and used without further refinement), was introduced into the interaction region by means of a heated effusive oven.[48] The oven was heated to approximately 66 °C, with the tip of the oven at 104 °C to ensure that there was no build-up of sample in the capillary. This produced a consistent background pressure in the chamber of between $1.4–1.6 \times 10^{-5}$ mbar during operation, with a sample density of typically 1×10^{14} molecules/cm^3.

VUV-PEPICO: With regards to the VUV data, we obtained static dissociative photoionization data of *trans*-stilbene oxide at the VUV end station of the SLS synchrotron, using a double velocity-map-imaging (VMI) photoelectron photo-ion coincidence ('PEPICO') spectrometer.[49–51] Monochromatized synchrotron light was scanned in the range of 8 to 15 eV (in 5 meV steps)[27] and used to observe the onset of photon-induced dissociation channels. The sample was introduced into the spectrometer through heated piping connected to a sample reservoir, with the reservoir held at 53 °C and the piping at a higher temperature to avoid unwanted sample deposition and blockages. The ion arrival events in this measurement were selected by coincident electrons with low kinetic energy, creating a threshold ion spectrum.[30] Whilst only a sub-section of the results of this experiment are presented here, full VUV experimental results covering a larger range of photon energies will be published at a later date.

Acknowledgements

We acknowledge the Paul Scherrer Institut, Villigen, Switzerland for provision of synchrotron radiation beamtime at beamline X04DB of the SLS, during proposal 20171655. We thank P. Hemberger, A. Bodi, D. Schleier and I. Fischer for support during the SLS beamtime. The Potsdam group is funded by a Lichtenberg Professorship of the Volkswagen Foundation. J.M. is founded by a BMBF Verbundforschungsprojekt 05K16IP1. We acknowledge funding from the DFG through grant INST 336/112-1. Finally, we thank Dr. T.J.A. Wolf (SLAC National Accelerator Laboratory) for stimulating discussions. Open access funding enabled and organized by Projekt DEAL.

Conflict of Interest

The authors declare no conflict of interest.

Keywords: femtochemistry · mass spectrometry · photochemistry · small ring systems · stilbene oxide

[1] M. K. Phibbs, B. deB Darwent, E. W. R. Steacie, *J. Chem. Phys.* **1948**, *16*, 39–44.
[2] R. Gomer, W. A. Noyes Jr., *J. Am. Chem. Soc.* **1950**, *72*, 101–108.
[3] J. Friedrichs, I. Frank, *Chem. Eur. J.* **2009**, *15*, 10825–10829.
[4] G. W. Griffin, *Angew. Chem. Int. Ed. Engl.* **1971**, *10*, 537–547; *Angew. Chem.* **1971**, *83*, 604–613.

[5] B. E. Arney Jr., R. C. White, A. Ramanathan, L. Barham, S. Sherrod, P. McCall, P. Livanec, K. Mangus, K. White, *Photochem. Photobiol. Sci.* **2004**, *3*, 851–853.
[6] F. Cordova, L. J. Doriol, A. Ipatov, M. E. Casida, C. Filippi, A. Vela, *J. Chem. Phys.* **2007**, *127*, 164111.
[7] M. Huix-Rotllant, B. Natarajan, A. Ipatov, C. Muhavini Wawire, T. Deutsch, M. E. Casida, *Phys. Chem. Chem. Phys.* **2010**, *12*, 12811–12825.
[8] M. Kawasaki, T. Ibuki, M. Iwasaki, Y. Takezaki, *J. Chem. Phys.* **1973**, *59*, 2076–2082.
[9] B. C. Roquitte, *J. Phys. Chem.* **1966**, *70*, 2699–2702.
[10] B. Bigot, A. Sevin, A. Devaquet, *J. Am. Chem. Soc.* **1979**, *101*, 1095–1100.
[11] S. Linder, K. White, M. Palmer, B. Arney, R. White, *Tetrahedron Lett.* **2002**, *43*, 1169–1170.
[12] H. Kristinsson, G. W. Griffin, *Angew. Chem. Int. Ed. Engl.* **1965**, *4*, 868; *Angew. Chem.* **1965**, *77*, 859–860.
[13] I. J. Lev, K. Ishikawa, N. S. Bhacca, G. W. Griffin, *J. Org. Chem.* **1976**, *41*, 2654–2656.
[14] P. C. Petrellis, H. Dietrich, E. Meyer, G. W. Griffin, *J. Am. Chem. Soc.* **1967**, *89*, 1967–1969.
[15] G. A. Lee, *J. Org. Chem.* **1976**, *41*, 2656–2658.
[16] R. Huisgen, *Angew. Chem. Int. Ed. Engl.* **1977**, *16*, 572–585; *Angew. Chem.* **1977**, *89*, 589–602.
[17] T. Do-Minh, A. M. Trozzolo, G. W. Griffin, *J. Am. Chem. Soc.* **1970**, *92*, 1402–1403.
[18] R. B. Woodward, R. Hoffmann, *J. Am. Chem. Soc.* **1965**, *87*, 395–397.
[19] R. B. Woodward, R. Hoffmann, *Angew. Chem. Int. Ed. Engl.* **1969**, *8*, 781–932.; *Angew. Chem.* **1969**, *81*, 797–870.
[20] L. E. Manring, K. S. Peters, *J. Am. Chem. Soc.* **1984**, *106*, 8077–8079.
[21] M. Lipson, B. C. Noll, K. S. Peters, *J. Org. Chem.* **1997**, *62*, 2409–2413.
[22] R. S. Becker, J. Kolc, R. O. Bost, H. Kietrich, P. Petrellis, G. Griffin, *J. Am. Chem. Soc.* **1968**, *90*, 3292–3293.
[23] R. S. Becker, R. O. Bost, J. Kolc, N. R. Bertoniere, R. L. Smith, G. W. Griffin, *J. Am. Chem. Soc.* **1970**, *92*, 1302–1311.
[24] J. González-Vázquez, L. González, E. Samoylova, T. Schultz, *Phys. Chem. Chem. Phys.* **2009**, *11*, 3927–3934.
[25] V. G. Stavros, J. R. R. Verlet, *Annu. Rev. Phys. Chem.* **2016**, *67*, 211–232.
[26] O. Ghafur, S. W. Crane, M. Ryszka, J. Bockova, A. Rebelo, L. Saalbach, S. De Camillis, J. B. Greenwood, S. Eden, D. Townsend, *J. Chem. Phys.* **2018**, *149*, 034301.
[27] M. Johnson, A. Bodi, L. Schulz, T. Gerber, *Nucl. Instrum. Methods Phys. Res. Sect. A* **2009**, *610*, 597–603.
[28] T. J. A. Wolf, D. M. Sanchez, J. Yang, R. M. Parrish, J. P. F. Nunes, M. Centurion, R. Coffee, J. P. Cryan, M. Gühr, K. Hegazy, A. Kirrander, R. K. Li, J. Ruddock, X. Shen, T. Vecchione, S. P. Weathersby, P. M. Weber, K. Wilkin, H. Yong, Q. Zheng, X. J. Wang, M. P. Minitti, T. J. Martínez, *Nat. Chem.* **2019**, *11*, 504–509.
[29] R. C. White, T. Rix, *J. Org. Chem.* **1987**, *52*, 2309–2311.
[30] K. Majer, R. Signorell, M. F. Heringa, M. Goldmann, P. Hemberger, A. Bodi, *Chem. Eur. J.* **2019**, *25*, 14192–14204.
[31] R. L. Asher, E. H. Appelman, B. Ruscic, *J. Chem. Phys.* **1996**, *105*, 9781–9795.
[32] F. Di Giacomo, *J. Chem. Educ.* **2015**, *92*, 476–481.
[33] B. Sztáray, A. Bodi, T. Baer, *J. Mass Spectrom.* **2010**, *45*, 1233–1245.
[34] A. L'Huillier, L. A. Lompre, G. Mainfray, C. Manus, *Phys. Rev. A* **1983**, *27*, 2503–2512.
[35] M. Koch, T. J. A. Wolf, M. Gühr, *Phys. Rev. A* **2015**, *91*, 1–5.
[36] M. Kotur, T. C. Weinacht, C. Zhou, K. A. Kistler, S. Matsika, *J. Chem. Phys.* **2011**, *134*, 184309.
[37] N. Kotsina, M. Candelaresi, L. Saalbach, M. M. Zawadzki, S. W. Crane, C. Sparling, D. Townsend, *Phys. Chem. Chem. Phys.* **2020**, *22*, 4647–4658.
[38] N. Kotsina, D. Townsend, *Phys. Chem. Chem. Phys.* **2017**, *19*, 29409–29417.
[39] S. Arslancan, L. Martínez-Fernández, I. Corral, *Molecules* **2017**, *22*, 998.
[40] W. Fuß, K. K. Pushpa, W. Rettig, W. E. Schmid, S. A. Trushin, *Photochem. Photobiol. Sci.* **2002**, *1*, 255–262.
[41] K. B. Clark, K. Bhattacharyya, P. K. Das, J. C. Scaiano, A. P. Schaap, *J. Org. Chem.* **1992**, *57*, 3706–3712.
[42] J. Franck, E. Rabinowitch, *Trans. Faraday Soc.* **1934**, *30*, 120–130.
[43] E. Tapavicza, I. Tavernelli, U. Rothlisberger, C. Filippi, M. E. Casida, *J. Chem. Phys.* **2008**, *129*, 124108.
[44] B. Bigot, A. Sevin, A. Devaquet, *J. Am. Chem. Soc.* **1979**, *101*, 1101–1106.
[45] W. C. Wiley, I. H. McLaren, *Rev. Sci. Instrum.* **1955**, *26*, 1150–1157.
[46] A. Giugni, S. Cavalieri, R. Eramo, L. Fini, M. Materazzi, *J. Phys. B* **2000**, *33*, 285–289.
[47] T. Okuno, T. Imasaka, Y. Kida, T. Imasaka, *Opt. Commun.* **2014**, *310*, 48–52.
[48] B. K. McFarland, N. Berrah, C. Bostedt, J. Bozek, P. H. Bucksbaum, J. C. Castagna, R. N. Coffee, J. P. Cryan, L. Fang, J. P. Farrell, R. Feifel, K. J. Gaffney, J. M. Glownia, T. J. Martinez, S. Miyabe, M. Mucke, B. Murphy, A. Natan, T. Osipov, V. S. Petrovic, S. Schorb, T. Schultz, L. S. Spector, M. Swiggers, F. Tarantelli, I. Tenney, S. Wang, J. L. White, W. White, M. Gühr, *J. Phys. Conf. Ser.* **2014**, *488*, 012015.
[49] A. Bodi, P. Hemberger, T. Gerber, B. Sztáray, *Rev. Sci. Instrum.* **2012**, *83*, 083105.
[50] B. Sztáray, K. Voronova, K. G. Torma, K. J. Covert, A. Bodi, P. Hemberger, T. Gerber, D. L. Osborn, *J. Chem. Phys.* **2017**, *147*, 013944.
[51] A. Bodi, B. Sztáray, T. Baer, M. Johnson, T. Gerber, *Rev. Sci. Instrum.* **2007**, *78*, 084102.

Manuscript received: April 14, 2021
Accepted manuscript online: May 26, 2021
Version of record online: June 17, 2021

